JOURNAL OF MATERIALS SCIENCE 8 (1973) 1765–1787

The impact strength of fibre composites

T. WILLIAMS
ICI Corporate Laboratory, Runcorn, Cheshire

G. ALLEN, M. S. KAUFMAN
Chemistry Department, The University of Manchester, Manchester

Two models have been developed which predict the crack initiation energy, notched impact strength and unnotched impact strength of fibre composites. One is applicable to composites containing short fibres and the other to composites containing long fibres. Data obtained with randomly oriented short fibre composites were consistent with the one model. The other model has been verified using composites containing uniaxially oriented long fibres and long fibres oriented randomly in a plane. The success of the model demonstrates that the high notched impact strength with long fibres is due to the redistribution of stress away from the stress concentrating notch, the extra stress that can be held by the fibre relative to the matrix and the work required to pull fibres out of the matrix during crack propagation. The parameters which have been shown to control the fracture energy are composite modulus, fibre length, fibre volume fraction, effective fibre diameter, fibre tensile strength and the coefficient of friction during fibre pull-out from the matrix. The matrix toughness on the other hand usually has no effect at all for composites containing fibres randomly oriented in two dimensions and only a minor effect in exceptional cases. The shear strength of the fibre-matrix bond has only an indirect effect in that it controls the number of fibres which pull out rather than fracture.

1. Introduction

The impact strength of a material is defined as the energy required for fracture across unit cross-section during high speed loading It gives a measure of the ability of the material to withstand impact loading and is important since articles are frequently subjected to such loading during service. In practice, the actual numerical value will depend upon the type of test and shape of the sample. The presence of surface flaws or notches also considerably lowers the impact strength of most homogeneous materials. Many impact tests have been devised, but one of the simplest and most widely used is the Charpy notched impact test [1]. It can give useful information about the in-service performance of different materials, especially if the notch tip radius is varied.

Improvement in the impact strength of some polymeric materials is highly desirable. Thus there is considerable interest in rubber-toughening glassy polymers such as polystyrene and polymethyl methacrylate which normally break in a brittle manner absorbing little energy. Despite a fall in the modulus associated with the incorporation of rubber, rubber-toughened polystyrenes are now well established commercially. HIPS and ABS, two commercial toughened polystyrenes have the toughening-rubber distributed in approximately spherical particles throughout the glassy matrix. Work has also been carried out on more novel toughened polymethyl methacrylate systems. These interstitially-polymerized materials consist of predominantly glassy polymer particles embedded in a continuous rubbery matrix. Properties of such materials are comparable with toughened polystyrenes, i.e. large increases in toughness are possible, but only at the expense of the stiffness of the system. The loss in stiffness of such systems limits their applicability.

It has been pointed out [2] that the NIS (notched impact strength) of fibre composites can be much larger than the NIS of each of the individual phases. An alternative method of toughening a polymer would therefore be to

incorporate fibres. As opposed to rubber-toughening, fibre-toughening would be achieved without any decrease in modulus, tensile strength or softening temperature. Indeed, fibre reinforcement is conventionally used to improve these properties. Published theoretical work predicting the mechanical properties of fibre composites is not comprehensive. The factors influencing both modulus and strength are well understood and theories are quite well developed though they are not yet completely adequate especially in the case of composites containing short randomly oriented fibres [4, 5]. The origin of the fracture energy of fibre composites is not so clearly resolved and a number of mechanisms have been suggested. Almost all theories to date have been concerned with uniaxially-oriented fibre composites. Most emphasis has been given to the consideration of the contribution of frictional work during fibre pull-out [6, 7]. Calculations of the energy required to de-bond the fibre from the matrix [2] and the flexural energy adsorbed up to failure have also been made [8]. In an alternative approach it is assumed that fibre-matrix bonding remains intact and work is done in the plastic deformation of the matrix material [9].

Theories predicting the fracture energy of composites containing random fibres have received little attention. Recent work [10] has shown that the impact strengths of random fibre composites are similar to those of oriented fibre samples. In order to explain this surprising result, extra energy absorption effects were postulated which would not occur for aligned fibres. These are: enhancement, during pull-out, of friction near the exit point of the fibre from the matrix; fragmentation of the matrix to allow pull-out of non-aligned stiff fibres and plastic bending deformation of fibres during pull-out. The extent to which these will occur is uncertain and will certainly vary with the properties of fibre and matrix components. Exact calculation is therefore difficult. It was shown, however, that the plastic bending energy could reach significant levels under favourable circumstances.

In this paper, an analysis is presented which predicts the notched and unnotched impact strength of composites containing both random and uniaxially-oriented long fibres. Good agreement has been obtained with results for composites made with long fibres of different types, diameters and concentrations and matrices of different toughness. A corresponding analysis for composites containing short fibres is also consistent with experimental results obtained on composites of the appropriate specification. For completeness, more qualitative results of a damage initiation test have also been carried out. These demonstrate that permanent damage (fibre-matrix de-bonding and limited crack propagation) can occur for impacting energies well below the fracture energy. In many applications this will limit the use of fibre composites. Emphasis in all of this work has been given to composites containing randomly-oriented fibres since previously these have received least attention.

2. Experimental

2.1. Sample preparation

Fibre composites with polymethyl methacrylate (PMMA) and rubber-toughened PMMA matrices were most widely used in this investigation. They were prepared by polymerization of the matrix around the fibres in a flat plate mould.

Methyl methacrylate (BDH laboratory grade) was first freed from water and inhibitor by refluxing over calcium hydride followed by distillation under reduced pressure. Azobisisobutyronitrile was used in the purity supplied by Genitron for initiation of the vinyl polymerization. Concentrations of 0.2% in the methacrylate were found to be adequate.

The preparation of PMMA toughened with polyurethane rubbers is described fully elsewhere [11]. The rubber precursors used in this study were methylene *bis* (4-phenyl isocyanate), purified by vacuum distillation, and poly(oxypropylene glycol), molecular weight 2000 (Daltocell B56) together with an equal amount of the appropriate glycol derivative of molecular weight 3000 (Daltocell T56) both purified by vacuum drying with a nitrogen bleed at 120°C for 2 to 3 h. Dibutyltindilaurate supplied by Alpha Inorganics Inc was used to initiate rubber gelation.

Moulds for composite fabrication were formed by two flat sheets of glass separated by a flexible gasket of Butyl rubber (Esso Chemicals). Fibres were arranged in the mould in the desired configuration, i.e. either randomly or uniaxially-oriented. The mould was sealed (except for a small gap in the gasket to be used for addition of monomer) by compression in a hot press and clamping with spring clips. De-gassed liquid monomer or monomer and rubber precursors were then poured into the mould. Trapped air bubbles were removed by holding the mould

under vacuum in a vacuum oven for a few minutes. The mould was then removed from the oven and completely sealed.

For rubber-toughened matrices, the moulds were left for 24 h at room temperature during which time the rubber precursors cross-linked to form a continuous network of polyurethane rubber. The mould was then kept at 50°C for 48 h, 70°C for 4 h, 90°C for 2 h and 120°C for 1 h to completely polymerize the vinyl phase. The matrix thus formed, consisted of spherical domains of PMMA of about 1000 Å diameter embedded in a continuous polyurethane (PU) network [12]. The proportion of PMMA to PU was controlled by the concentration of rubber precursors in MMA in the original mixture. With PMMA matrices, of course, the initial room-temperature gelation period was not required. When polypropylene fibres were used, a final curing temperature of 90°C and not 120°C was used to eliminate the possibility of changing the fibre properties during fabrication.

A few composites were prepared by a conventional compression moulding technique using cold-cured polyester and epoxy matrices. Scott-Bader Crystic 199 with accelerator E and catalyst paste H and Shell Chemicals Epikote 828 and Epikure RTV were used for these samples. The edges were sealed with strips of Butyl 365 rubber. Fibres were laid in the mould and an excess of de-gassed matrix precursors were added. After rolling and dabbing the fibres to remove air bubbles, the samples were cured at room temperature under pressure in a press.

A wide range of fibre types was used with the different matrices. These were:

(i) water-sized E glass (i.e. with no surface coating) supplied by Fibreglass Ltd;

(ii) several E glass fibre samples with different diameters and numbers of filaments per bundle supplied by Owens-Corning Fiberglas Ltd;

(iii) chopped E glass fibre samples with various lengths, diameters and numbers of filaments per bundle, all coated with a size of PVA containing additives A174 and A1100 which make the fibres compatible with vinyl matrices. These fibres were kindly supplied by Fibreglass Ltd;

(iv) Ulstrom highly-drawn polypropylene fibre (228 filaments, total decitex 1254, reference number 1140-228-U 100)*;

(v) H-type Terylene, highly-drawn polyethylene terephthalate fibre (192 filaments, 1000 total decitex, reference 1000/192-Bright 655H)*;

(vi) L3-type Terylene, medium tenacity chopped fibre (4.4 decitex per filament). Fibre lengths were 0.06, 0.6, 1.2 and 10 cm*;

(vii) as-spun Terylene fibre (i.e. undrawn);

(viii) Terylene "macro-fibre", highly-oriented, large diameter fibres (7 filaments, 4900 total decitex)*;

(ix) Nylon 6.6 fibre (single filament, 17 decitex)*;

(x) spun cotton fibre, supplied by English Sewing Ltd;

(xi) Lycra 124 and 126 elastomeric fibres, supplied by DuPont;

(xii) woven E glass fabric (5/2/225/E) supplied by Fothergill and Harvey.

Terylene, nylon and Ulstron fibres were very kindly supplied by ICI Fibres Division.

Except possibly in the case of the shortest fibres used (0.06 cm L3 Terylene), all fibres were aligned in the plane of the sheet by the fabrication method selected.

2.2. Impact testing

A Hounsfield Plastics Impact Tester was used. Samples for Charpy notched impact testing [1], 50 mm × 6 mm × 3 mm, were cut from the cast sheets and notched with a cutter of tip radius 0.25 mm. Depth below the notch was 3.8 mm in each case. At least six samples were tested from each sheet and the average NIS determined. In addition to room temperature measurements, a selected number of samples were tested over a very wide temperature range (−196 to +120°C). The sample was housed in a small oven/refrigerator which controlled the temperature to $\pm \frac{1}{2}$°C. When equilibrium had been reached (after about 30 min), the sample was removed and tested. Testing was carried out within 3 sec of removal from the oven. Errors in temperature due to a change after removal from the oven were small and do not alter significantly the conclusions drawn from these results.

Similar samples to the ones used for notched testing were cut from the cast sheets for Charpy unnotched testing [1] and damage initiation

*The decitex of a fibre is the weight in grams of a 10 000 m length of fibre.

testing. Instead of notching, the cut edges of the samples were polished more carefully. For the damage initiation test, the samples were mounted so that one of the faces originally in contact with the mould plate was struck by the pendulum. (In the Charpy notched and unnotched tests cut, polished edges were struck.) A pendulum of smaller weight than for unnotched testing was used. After being struck by the pendulum, the sample was carefully examined by eye for signs of damage. If the sample was still not broken, the test was repeated several times and inspected for damage after each impact. Different samples cut from the same sheet were tested with pendulums of different weights so that the progressive change in damage with increase in pendulum weight could be documented. At least three samples were tested with each weight to check the representative nature of the observations. Such a test is, of course, subjective. For example, different observers may detect debonding at slightly different input energies. In addition there is a large scatter between different samples. Nevertheless the trends in the observation are valid. To enable small changes in pendulum weight to be investigated, extra weights were fixed with tape to several of the pendulums. This was not usually necessary for the fibre composites because of the wide range in pendulum weight over which damage progressively increased. For comparison with NIS and UNIS data, input weights were converted to an equivalent input energy and divided by the area of cross-section of the sample. Input energies per unit area were quoted in units of kJM^{-2}.

2.3. Tensometer simulation of Charpy tests

A Hounsfield 3-point bending rig was modified to give 4-point bending with exactly the same loading geometry as used in the Charpy impact test. Charpy test specimens were held in this rig and tested on an E-type Hounsfield Tensometer at cross-head speeds of 0.5, 1 and 5 in. min^{-1}. This experiment gives a record of the force on the cross-head against cross-head movement, i.e. the force on the centre of the span against the central span deflection. A representative range of samples were tested in this manner to check each stage in the theory developed for predicting the fracture energy.

The energy required to bend the Charpy sample up to the maximum stress is a measure of the energy required before crack initiation, i.e. the crack initiation energy E_i. The area under the rising force region of the tensometer curve therefore gives a direct measure of E_i at the tensometer strain rate. The total area under the curve gives the total fracture energy E_t absorbed in failure at the tensometer strain rate. For comparison with NIS data, E_i and E_t were divided by the sample area under the notch and the results, e_i and e_t, evaluated in units of kJm^{-2}. Values of e_i, e_t and F/b (the force on the centre span at failure, divided by the sample width) were found to be independent of testing speed in the range with which the tensometer could be reliably used (see Table I). The results suggest that it may be possible to ignore the difference in the rate of the Charpy and tensometer tests. Confirmation is given by the good correlation between e_t and NIS values for a wide range of types of fibre composite (Table I). The tensometer measurements e_i can therefore be used as a measure of the crack initiation energies occurring in the impact test.

2.4. Flexural modulus

A conventional 3-point bend test was used to determine the flexural moduli. The span-to-depth ratio was 16 for randomly-oriented fibres and 30 for uniaxially-oriented fibres. A tensometer cross-head speed of 0.21 in. min^{-1} was used.

2.5. Fibre concentration

The weight of fibre in a known weight of composite, and hence the fibre weight fraction W_f, was determined with pieces produced by impact testing. The matrix polymer was dissolved away by repeated washing with chloroform in a Soxhlet extraction apparatus. Results were consistent with values determined by matrix burn-off for the glass fibre composites. With composites of polymer fibres in epoxy and polyester matrices neither solvent extraction nor burn-off could be used. In these cases, an approximate estimate of W_f was taken as the ratio of fibre used in composite fabrication to the total composite weight.

The fibre volume fraction V_f in the composite was calculated from W_f using the equation

$$V_f = \frac{W_f(d_m/d_f)}{1 - W_f[1 - (d_m/d_f)]}$$

where d_m and d_f are the densities of the matrix and fibre respectively.

2.6. Single fibre pull-out tests

Single fibre pull-out tests were carried out by

TABLE I Results of tensometer simulation of Charpy impact test

Matrix	Fibre	Fibre length (cm)	W_f (%)	Fibre orientation	Cross-head speed (in min^{-1})	F/b (MN m^{-1}) $\times 10^{-2}$ ($\pm$ 6%)	e_i (kJ m^{-2}) ($\pm$10%)	e_t (kJ m^{-2}) ($\pm$ 10%)	Charpy NIS (kJ m^{-2})
PMMA	L3	0.06	31	random	0.5	1.9	3.2	4.4	4.3 $\pm$ 1
	Terylene				5.0	1.9	3.2	5.2	4.3 $\pm$ 1
PMMA	L3	1.3	42	random	0.5	2.0	8.0	24.0	25 $\pm$ 9
	Terylene				5.0	2.5	11.6	28.0	25 $\pm$ 9
PMMA	glass	0.6	55	random	0.5	8.5	17.3	48.0	45 $\pm$ 7
					5.0	9.5	16.7	42.0	45 $\pm$ 7
PMMA/PU	woven	continuous	48	woven-2D	1.0	7.4	4.5	36.0	53 $\pm$ 6
	glass				5.0	5.0	4.5	27.0	53 $\pm$ 6
epoxy	Ulstron	continuous	18	uniaxial	0.5	4.0	24.0	—	90 $\pm$ 26
					5.0	3.4	22.0	—	90 $\pm$ 26
PMMA	L3	1.3	47	random	5.0	3.7	16.0	36.0	37 $\pm$ 10
PMMA	L3	1.3	36	random	5.0	2.6	7.0	22.0	24 $\pm$ 7
PMMA	L3	0.6	48	random	5.0	3.2	6.0	28.0	24 $\pm$ 5
PMMA	L3	2.5	17	random	5.0	3.2	11.5	19.5	20 $\pm$ 2.5
Polyester	L3	10.0	11	random	5.0	2.8	9.3	17.5	13.6 $\pm$ 2.8
PMMA	glass	continuous	42	uniaxial	5.0	13.4	37.0	62.0	56 $\pm$ 16
PMMA	glass	0.6	47	random	5.0	—	24.0	36.0	27 $\pm$ 6
PMMA	glass	2.5	40	random	5.0	10.9	23.0	44.0	72 $\pm$ 7
PMMA	glass	0.6	47	random	5.0	5.4	9.0	34.0	32 $\pm$ 2
PMMA	glass	0.6	39	random	5.0	5.2	7.0	31.0	56 $\pm$ 9
PMMA	glass	0.6	52	uniaxial	5.0	10.5	22.0	44.0	64 $\pm$ 15
PMMA	H-terylene	10.0	19	random	5.0	5.0	23.0	56.0	69 $\pm$ 10
polyester	cotton	10.0	14	random	5.0	1.5	3.5	7.0	8 $\pm$ 1.5
PMMA	cotton	5.0	17	random	1.0	2.3	5.6	9.1	7.6 $\pm$ 2.8

J. D. Emmerson [13] in a separate study. The principle of the method adopted has already been described [14]. Samples for testing are more easily prepared with cold-setting resins and for this reason polyester and epoxy matrices were used. Individual fibre filaments were mounted with a portion embedded in a drop of matrix suspended from a wire. The force necessary to pull the fibre from the matrix was measured using a tensometer. The force increased until the fibre-matrix bond failed. In general, after failure of the bond a smaller force was observed; it was required to overcome frictional forces exerted on the fibre as it was pulled out from the matrix. Two interfacial adhesion coefficients could therefore be obtained from each test: the adhesive shear strength of the fibre-matrix bond τ_s and the interfacial frictional coefficient τ_f. At least six pull-out tests were carried out with each fibre matrix system and average values for τ_f and τ_s determined.

2.7. Single fibre tensile testing

The initial modulus, failure stress and failure strain for fibres used in this investigation were determined with a tensometer using conventional fibre tensile testing procedure. The tested initial length (gauge length) was 10 cm with a tensometer cross-head speed of 2 cm min^{-1}.

Fibre properties are listed in Table II together with their adhesive coefficients determined in epoxy and polyester matrices.

3. Qualitative observations of failure process

For most fibre composites investigated, failure in the notched impact test occurred by a crack which propagated from the notch tip across the width of the sample (Fig. 1a). In many cases, especially with large fibre loadings and the higher strength fibres, the sample was not completely fractured into two pieces; fibres near the compressive face tended to hold the sample together (Fig. 1b). The fracture surfaces of all composites showed considerable fibre pull-out with maximum pull-out lengths varying from 0.03 to 0.5 cm. These lengths were measured for each

TABLE II Fibre tensile properties and adhesive coefficients in epoxy and polyester matrices

Fibre	Diameter (μm)	Fibre tensile strength (MN m^{-2})	Fibre failure strain (%)	Fibre tensile modulus ($\times 10^3$ MNm^{-2})	Epoxy matrix		Polyester matrix	
					τ_s (MN m^{-2}) ($\pm$ 50%)	τ_f (MN m^{-2}) ($\pm$ 50%)	τ_s (MN m^{-2}) ($\pm$ 50%)	τ_f (MN m^{-2}) ($\pm$ 50%)
Water-sized "E" glass	11.5	3400	4.5	69	18.4	—	14.0	—
H-type Terylene	23.3	920	14	16	8.9	3.4	17.1	3.1
L3-type Terylene	19.8	520	13	9	6.4	2.7	14.8	3.6
Ulstron	30.0	570	24	7.7	5.2	2.4	2.5	2.6
Cotton	—*	590	5.0	8.3	5.8	2.0	0.63	0.75
Nylon	11.3	610	30	4.2	—	—	—	—

*Each cotton filament (diameter approximately 290 μm) contained many fibrils of approximately 10 μm diameter.

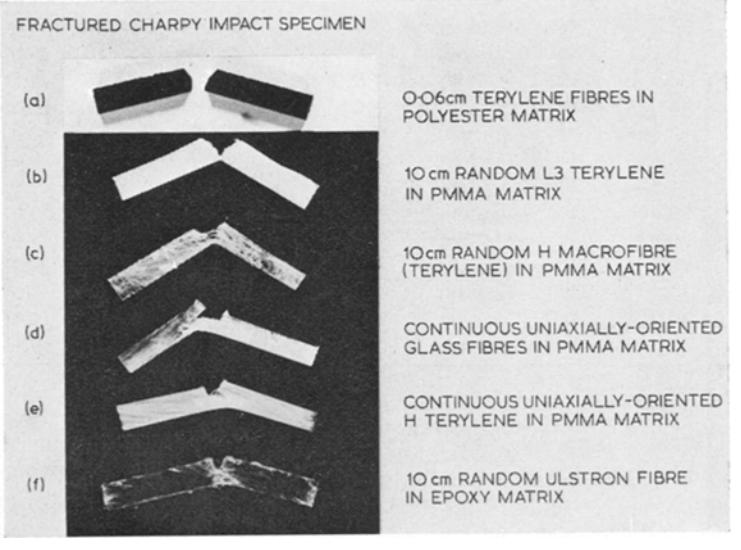

Figure 1 Fractured Charpy impact specimen. (a) 0.06 cm L3 Terylene fibres in polyester. (b) 10 cm planar random L3 Terylene in PMMA. (c) 10 cm planar random H Terylene macro-fibre in PMMA. (d) Continuous uniaxially-oriented glass fibres in PMMA. (e) Continuous uniaxially-oriented H Terylene in PMMA. (f) 10 cm planar random Ulstron fibres in epoxy.

sample either from scanning electron micrographs or visually. Despite the approximate measurement technique the precision was still greater than possible errors resulting from judgement of the length corresponding to the maximum pull-out length and the variation from sample to sample.

The fracture surfaces of random fibre composites are very disordered and little information can be obtained from scanning electron micrographs (e.g. Fig. 2a and b). In a few cases when long, high strength fibres with large diameter or weak bonding were used, partial fibre pull-out occurred with no sign of fibre fracture. In these cases after failure the matrix was often completely broken into two components but fibres bridged the gap between the components (Fig. 1c).

Composite samples with continuous fibres oriented along the Charpy specimen length had a greater resistance to crack propagation across the sample width. There was a tendency for cracks to travel parallel to the fibres before traversing the width (Fig. 1d). A typical scanning electron micrograph for a continuous uniaxially oriented glass fibre sample is shown in Fig. 2c. The variation in pull-out length is obvious as well as the non-uniform distribution of fibres across the sample and presence of some misaligned fibres.

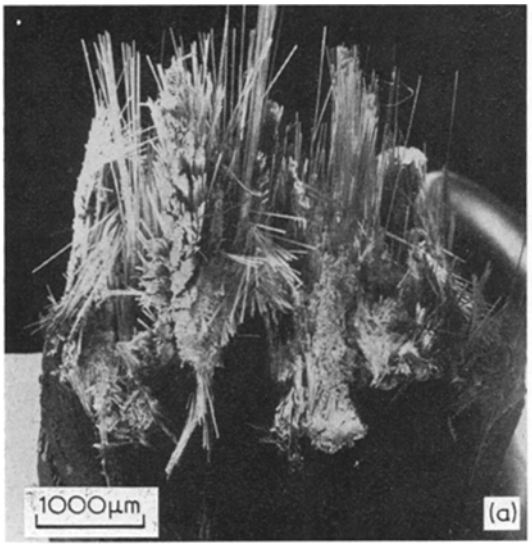

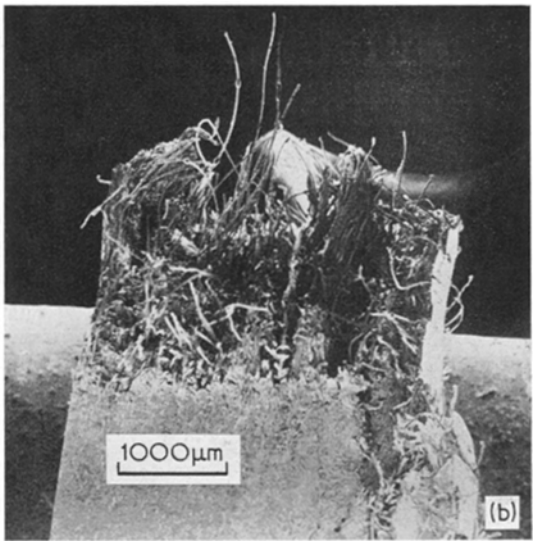

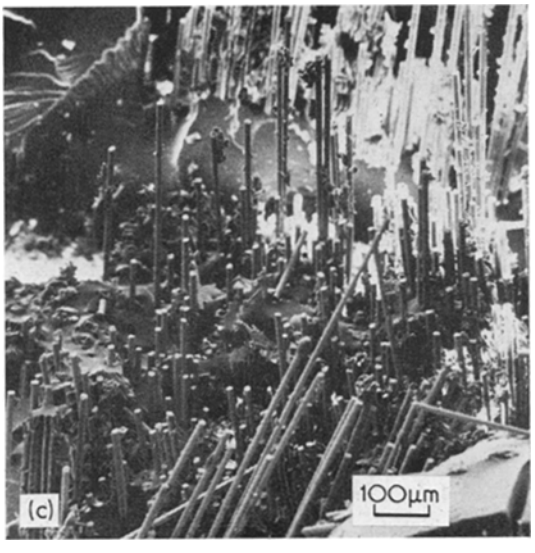

Figure 2 Scanning electron micrographs of fracture surfaces. (a) Random glass fibres/PMMA matrix. (b) Random L3 Terylene/PMMA matrix. (c) Uniaxially-oriented glass fibres/PMMA matrix.

The latter two defects are likely to occur in commercial samples to the same sort of extent as in our case and so no great effort was made to reduce them.

Continuous, uniaxially-oriented strong polymer fibres which fail at larger strains than glass fibres gave composites with even greater resistance to crack propagation across the width. At low concentrations, limited propagation did occur but a far larger proportion of the width was not fractured before the sample bent sufficiently to allow it to leave the test instrument. At high-fibre concentrations, crack propagation across the width was entirely restricted (Fig. 1e). A crack was formed along the fibres from the notch and the sample bent until it could leave the test instrument. Many small cracks were visible in the matrix throughout such samples after testing, but it was apparent that the tough polymer fibres had successfully stopped each of these from developing. The high crack-stopping ability of polymer fibres was particularly evident with Ulstron fibre composites. Little crack propagation was observed, even with only moderate concentrations (i.e. as low as 20% fibre) of random fibres. In these cases samples failed by buckling of the compressive face (Fig. 1f). This mode of failure was associated with high energy absorption.

4. Analysis of the NIS of fibre composites

In this section methods are presented for calculating the NIS values of fibre composites. The approach involves a number of independent calculations and assumptions. Each stage will be compared with experimental data and discussed immediately after presentation.

4.1. Failure stress and strain

4.1.1. Theory

Before predicting the initiation energy e_i it is necessary to be able to predict the fibre com-

posite failure stress σ_c. Four different failure stresses can be calculated and the one applicable will depend upon the failure mechanism.

Failure by interlaminar shear along the neutral axis was not observed during impact testing. This failure mode will not therefore be considered further.

Failure could start when the matrix reaches its tensile strength σ_m. The extra load supplied to the fibres could then result in complete composite failure. If the ratio of fibre length to diameter is sufficiently large to enable load transfer from matrix to fibre to reach the limit set by uniform strain conditions, then the failure strain (ϵ_c), for this mode of failure would be equal to the matrix failure strain ϵ_m, i.e.

$$(\epsilon_c)_1 = \epsilon_m. \tag{1}$$

The composite failure stress $(\sigma_c)_1$ when the matrix is at a stress σ_m is given by

$$(\sigma_c)_1 = \sigma_m (E_c/E_m) \tag{2}$$

where E_c and E_m are the composite and matrix moduli.

In an alternative failure mode, the composite fails when the fibres fracture. As above, if fibres are sufficiently long and uniform strain conditions hold, then the composite failure stress $(\sigma_c)_2$ is given by

$$(\sigma_c)_2 = \sigma_f (E_c/E_f) \tag{3}$$

where σ_f and E_f are the fibre tensile strength and modulus respectively. Equation 3 is equivalent to the simple, widely-used equation for composite tensile strength [3]. In this form, however, the equation is independent of the fibre-orientation distribution. Use of experimentally determined moduli may compensate, to some extent, errors due to a departure from uniform strain conditions, which could be the major source of error in the theory.

For this second mode of failure the failure strain $(\epsilon_c)_2$ is equal to the fibre failure strain

$$(\epsilon_c)_2 = \epsilon_f. \tag{4}$$

Equations 3 and 4 imply that fracture occurs when the maximum fibre stress in the random fibre composite (i.e. the stress in the fibres which are oriented in the stress direction) is equal to the fibre strength. Fibres at other orientations have lower stresses at this point. However, after the oriented fibres have failed, extra stress will be quickly transferred to these other fibres and the stress in them will rise to σ_f with little change in the total stress in the composite.

In the third possible mode of failure, the matrix at the notch tip starts to crack, but fibres stop crack-propagation by carrying some of the stress. Eventually the stress in the fibres rises to such an extent that complete de-bonding and pull-out of fibres occurs and the crack propagates. Fibre pull-out, rather than fracture, will occur when interfacial shear strength and fibre length are sufficiently small so that the force resisting complete fibre pull-out cannot rise to the fibre tensile strength. As with fibre fracture, fibres oriented in the stress direction will start to pull out before fibres at other orientations. It is proposed that the component of stress along the other fibres will rise and they will eventually start pulling out at the same fibres stress as if they were oriented in the stress direction. The maximum stress that an individual fibre can maintain before pull-out is given by

$$\sigma_{fp} = 4l\tau_s/d \tag{5}$$

where l is the length of fibre resisting pull-out and d is the fibre diameter. Now in a composite, l will vary from zero up to the maximum observed pull-out length l_m. The adhesive bond for fibres with low l values will be broken at low loads. These fibres will then only contribute a stress

$$\sigma_{fp} = 4l\tau_f/d. \tag{6}$$

Eventually all but the very few fibres with the maximum values of $l(= l_m)$ will have a stress contribution predicted by Equation 6. At the failure point the longest fibres will start to de-bond. The fibre stresses will then vary from zero up to just less than $4l_m\tau_f/d$, with an insignificant proportion at a stress of $4l_m\tau_s/d$. The mean fibre stress at the point of maximum stress of fibres oriented along the stress direction will, therefore, be

$$\sigma_{fp} = 2l_m\tau_f/d. \tag{7}$$

If we assume that, although the fibres are short enough to pull out, their aspect ratio is large enough for uniform strain conditions then the composite stress $(\sigma_c)_3$ for this maximum average fibre stress can be calculated:

$$(\sigma_c)_3 = (E_c/E_f)(2l_m\tau_f/d). \tag{8}$$

For a linear composite stress-strain curve up to the fibre pull-out point, the failure strain is given by:

$$(\epsilon_c)_3 = (\sigma_c)_3/E_c = 2l\tau_f/d\,E_f. \quad (9)$$

Transition from failure mode 2 to mode 3 for fibre of length L will be governed by Equation 5, with the maximum possible pull-out length given by $L/2$. All fibres will pull-out if

$$\sigma_{fp} = 2L\tau_s/d < \sigma_f. \quad (10)$$

As soon as the calculated value of σ_{fp} exceeds σ_f, some fibre will fracture. However, others will have l values close enough to the line of crack propagation for pull-out to occur before fracture. Hence the average stress at fracture in the fibres oriented along the stress, will only become close to σ_f for fibres with L, τ_s and d such that σ_{fp} calculated is much greater than σ_f. A gradual transition from fracture energies predicted with mode 2 to the ones predicted with mode 3 would be expected.

In order to test each of the above theories, the fracture stress and strain must be related to the force F on the centre span and the centre span deflection χ at failure in the tensometer experiments. Let us assume that the fibres spread the load away from the notch, eliminating any stress intensification. Any de-bonding between fibre and matrix will certainly enhance this tendency. The maximum stress and strain can then be related to F and χ by the standard formulae for bending beams:

$$F/b = \frac{U^2}{1.5D}\sigma_c \quad (11)$$

and

$$\chi = \frac{D^2}{6U}\epsilon_c \quad (12)$$

where b is the sample width, U the depth below the notch and D the span.

These equations assume that the sample deflection is small compared with the span [15]. In fact, the deflection at peak load was sufficiently small for all samples so that Equations 11 and 12 should be accurate within 5%. Some error in the expected force/deflection curves only arises for continuous uniaxially-oriented polymer fibre composites which carry large stresses at very large deflections. In these cases, only the qualitative features were of interest.

4.1.2. Comparison with results

The variation in failure strain with fibre type (Table III) suggests that the failure mode is governed by fibre or interface failure and not by matrix failure. Experiments with matrices of different toughness (and different failure strains) also support this conclusion: NIS values observed for planar random fibre composites (Fig. 3) and the failure strain of composites (Table III) were found to be independent of the matrix material.

Theoretical values of F/b for a wide range of fibre composites have been calculated using Equations 3 and 11, i.e. assuming fibre fracture determines the maximum composite stress and

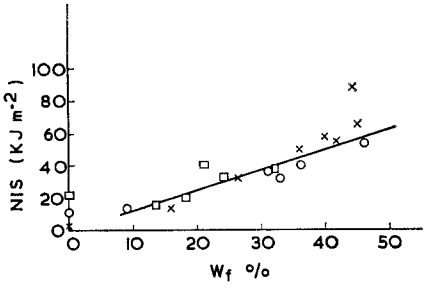

Figure 3 Effect of matrix toughness on NIS of composite containing planar random glass fibres of length 1.3 cm. Toughness of unfilled rubber toughened PMMA matrix is indicated by the $W_f = 0\%$ points.

TABLE III Failure strains observed in tensometer simulation of Charpy test and comparison with theoretical values

Fibre	Matrix	ϵ_c (%) ($\pm$ 10% of ϵ_c)	ϵ_f (%)	ϵ_c (theoretical)* (%)
"E" glass fibre	PMMA	5.2	4.8	5.0
	polyester	5.5	4.8	5.0
	epoxy	4.1	4.8	5.0
L3 Terylene	PMMA	6.9	13.0	6.0
	polyester	5.9	13.0	6.0
H Terylene	PMMA	6.8	14.0	6.0
Woven glass	PMMA	2.5	2.7	2.8
	PMMA/PU	2.5	2.7	2.8
	PAN/PU	2.9	2.7	2.8

*Calculated using Equation 13.

TABLE IV Comparison of long fibre theory (Section 4) with tensometer simulation and NIS data

Fibre type	Length (cm)	V_f (%)	F/b_{Th}* (MN m^{-1}) $\times 10^{-2}$	F/b_{expt}‖ (MN m^{-1}) $\times 10^{-2}$ ($\pm$ 6%)	χ_{Th}† (m) $\times 10^{-3}$
PMMA matrices					
L3 Terylene (random fibres)	0.06	27.5	2.7	1.9	2.6
	0.64	44.3	3.3	3.2	2.6
	1.27	38.4	1.6	2.5	2.6
	1.27	43.4	2.2	2.7	2.7
	1.27	33.1	3.7	3.6	2.6
	2.5	15.5	2.7	3.2	2.7
L3 Terylene (uniaxially-oriented fibres)	10.0	16.8	3.8	—	2.6
	1.27	37.2	6.6	5.0	2.6
H Terylene (random fibres)	10.0	17.2	5.0	4.9	2.6
Water-sized glass (random)	10.0	16.0	8.8	—	2.2
(uniaxially-oriented)	continuous	25.0	10.0	13.0	2.2
sized "E" glass (random)	2.5	33.0	10.7	10.9	2.3
Polyester matrices					
L3 Terylene (random fibres)	0.06	16.8	4.7	—	2.6
	0.64	12.3	5.2	—	2.6
	1.27	21.4	4.7	—	2.6
	10.0	8.7	3.2	2.8	2.6
H Terylene (random fibres)	10.0	27.0	5.2	—	2.6
H Terylene (oriented fibres)	continuous	19.0	6.6	—	2.6
Water-sized glass (random)	10.0	25.0	10.0	8.85	2.2
(oriented fibres)	continuous	9.5	5.4	6.45	2.2
Ulstron (random fibres)	10.0	26.0	4.6	5.6	3.1
	1.27	37.6	5.3	—	3.1
(oriented fibres)	continuous	26.0	9.6	—	3.3
Epoxy matrices					
L3 Terylene (random fibres)	0.64	17.0	3.1	—	2.6
	1.27	19.6	3.7	—	2.6
	10.0	17.0	3.7	—	2.6
H Terylene (random fibres)	10.0	26.0	4.5	—	2.6
Water-sized glass (random)	10.0	19.0	7.5	—	2.2
(oriented fibres)	continuous	15.4	16.1	8.0	2.2

*Calculated using Equations 3 and 11.
†Calculated using Equations 13 and 12.
‡Calculated using Equation 14.
§Calculated using Equation 19.
‖Data from tensometer simulation of Charpy test.

that the fibres completely eliminate the stress-concentrating effect of the notch. Results compare well with values determined experimentally in the tensometer experiment for both planar-random and uniaxially-oriented fibre composites with the exception of those containing the shortest fibres (Table IV). Fig. 4 summarizes this comparison between experiment and theory and demonstrates that despite the considerable simplifications and approximations in the theory, it can be used to predict the fibre composite failure stress for oriented and planar random fibre composites.

As expected, the composite failure strain was consistent with the fibre failure strain for glass fibre composites. With polymer fibres, however, samples failed at lower strains than expected. An alternative method of predicting E_c was therefore attempted. If it is assumed that the composite stress-strain curve is linear up to the fracture stress, the predicted failure stress and composite modulus can be used to predict the

χ_{expt} ‖ (m) $\times 10^{-3}$ (± 6%)	$(e_i)_{Th}$ ‡ (kJ m^{-2})	$(e_i)_{expt}$ ‖ (kJ m^{-2}) (± 10%)	e_{po} § (kJ m^{-2})	$(e_i)_{Th} + e_{po}$ (kJ m^{-2})	$(NIS)_{expt}$ (kJ m^{-2})
1.6	9.3	3.2	—	—	4.3 ± 1.0
—	11.3	—	40.0	51	24.3 ± 4.7
2.9	5.4	10.0	34.5	40	25.0 ± 4.0
2.6	7.8	16.0	27.0	35	37.0 ± 10.0
1.4	12.8	7.0	30.0	43	24.0 ± 7.0
2.5	9.5	11.5	14.0	23	19.9 ± 2.5
—	13.0	—	2.0	15	22.0 ± 5.0
3.1	23.0	14.0	33.5	56	26.0 ± 8.0
2.95	17.0	23.0	24.0	41	69.0 ± 10.0
—	26.0	—	8.0	34	33.0 ± 10.0
2.0	30.0	37.0	7.0	37	56.0 ± 16.0
1.5	24.0	23.0	47.0	70	72.0 ± 7.0
—	16.0	—	—	—	2.0 ± 0.2
—	18.0	—	1.3	19	4.0 ± 1.0
—	16.0	—	2.3	18	9.6 ± 2.0
2.6	11.2	9.3	2.3	13	13.6 ± 2.8
—	18.0	—	9.0	27	26.0 ± 11.0
—	23.0	—	5.0	28	44.0 ± 11.0
1.4	26.0	16.0	19.0	45	50.0 ± 12.0
2.4	17.0	27.0	8.3	25	44.0 ± 7.0
3.1	30.0	17.0	11.3	41	43.0 ± 10.0
—	21.5	—	56.0	77	41.0 ± 7.6
—	43.0	—	26.0	69	58.0 ± 10.0
—	10.8	—	—	—	4.4 ± 0.8
—	12.7	—	5.4	18	13.0 ± 5.0
—	12.7	—	5.4	18	11.5 ± 2.0
—	15.4	—	15.0	30	32.0 ± 6.0
—	22.0	—	13.2	35	33.0 ± 9.0
1.8	47.0	16.0	7.5	55	83.0 ± 24.0

composite failure strain:

$$\epsilon_c = (\sigma_c)_2/E_c. \quad (13)$$

Experimental and theoretical data were in much better agreement in this case (Table III). The discrepancy between the two theories is a result of the non-linear stress-strain curve of polymer fibres. The result indicates that the fibre fracture occurs in the composite with less, or more localized, fibre ductility owing to the constraining effect of the matrix.

With composites containing the shortest fibres (0.06 cm long Terylene) stresses and strains calculated assuming fibre fracture are much too large (Table IV). Fibre pull-out could therefore control the fracture in these cases. Calculations assuming the model discussed above, i.e. Equations 8, 9, 11, and 12, predict smaller stresses (Table V). The experimental data are too few to establish the model proposed, but they are not inconsistent with it.

4.2. Initiation energy e_i

From the theoretical estimates of the centre span force and deflections at composite failure, the flexural energy needed to bend the Charpy sample to the point where a crack initiates can be calculated.

Flexural energy to crack initiation per unit area under the notch,

$$(e_i)_{Th} = \tfrac{1}{2}F\chi/bu$$

TABLE V Short fibre composites: comparison of theory with tensometer simulation and NIS data

Matrix	Fibre type	Length (cm)	V_f (%)	F/b_{Th}* (MN m^{-1}) $\times 10^{-2}$	F/b_{expt}‖ (MN m^{-1}) $\times 10^{-2}$ ($\pm$6%)
PMMA	L3 Terylene (random)	0.06	27.5	0.9	1.91
Polyester	L3 Terylene (random)	0.06	16.8	1.1	1.22

*Calculated using Equations 8 and 11.
†Calculated using Equations 9 and 12.
‡Calculated using Equation 14.
§Calculated using Equation 15.

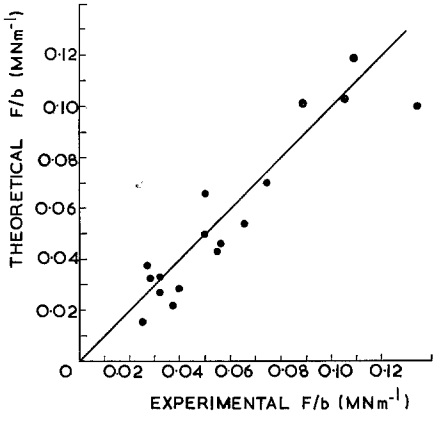

Figure 4 Comparison of theoretical and experimental failure forces per unit width.

i.e.

$$(e_i)_{Th} = (1/2u)\,(F/b)_{Th}\,(\chi)_{Th} \qquad (14)$$

assuming a linear force/deflection curve. $(e_i)_{Th}$ has been calculated for a wide range of fibre composites and can be seen to correlate with the experimental data for long-fibre composites (Table IV and Fig. 5). The theory is also shown to be equally applicable to planar-random or uniaxially-oriented fibre composites. Values calculated for very short randomly-oriented fibres are also consistent with experimental data (Table V).

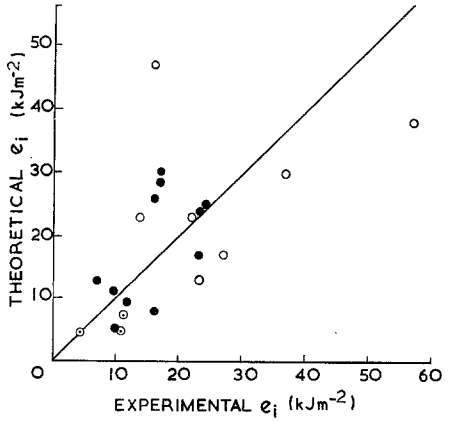

Figure 5 Comparison of theoretical and experimental initiation energies e_i for (●) random fibres, (○) uniaxially-oriented fibres and (⊙) woven glass cloth (2D orientation).

4.3. Pull-out energy e_{po}

Once crack propagation has started, a contribution to the crack propagation energy will come from the work done against friction in pulling fibres out of the opposite fractured face. For a distribution in pull-out lengths up to a maximum length l_m, the work of pull-out e_{po} is given by [7]

$$e_{po} = \frac{V_f \tau_f l_m^2}{3d} \cdot \qquad (15)$$

This expression is calculated in an identical manner to the example given in Appendix 2 in which thin rectangular fibres are considered. It assumes that the sample is completely fractured. For samples which did not break into two pieces during the impact test there will be a small error due to the reduced fracture surface area. In all cases, however, the error due to this effect was small and has been neglected. It is also assumed that all fibres are oriented along the stress direction. Now the frictional forces which oppose pull-out will always act along a fibre. Thus, regardless of orientation, fibres will not pull-out until the stress in the fibre reaches the value appropriate for uniaxial fibres. Of course for fibres oriented almost along the crack direction, failure in tension at the fibre-matrix interface will occur and not fibre pull-out. However, provided only a small proportion of fibres are oriented near the plane of the crack it is to be expected that Equation 15 will still predict e_{po} for all orientation distributions. The similarity between oriented and random fibre composite impact strengths is not therefore surprising and extra energy absorption mechanisms for random composites need not be sought to explain this observation [10].

With long fibre composites, l_m should be

χ_{Th}† (m) $\times 10^{-3}$	χ_{expt}‖ (m) $\times 10^{-3}$ (±6%)	$(e_i)_{Th}$‡ (kJ m^{-2})	$(e_i)_{expt}$‖ (kJ m^{-2}) (±10%)	e_{po}§ (kJ m^{-2})	$(e_i)_{Th} + e_{po}$ (kJ m^{-2})	$(NIS)_{expt}$ (kJ m^{-2})
0.88	1.60	1.1	3.2	1.3	2.4	4.3 ± 1.0
0.62	0.95	0.9	1.5	1.0	1.9	2.0 ± 0.15

‖Data from tensometer simulation of Charpy test.

related to the fibre tensile strength σ_f and the interfacial adhesive bond τ_s by the equation

$$l_m = \frac{d\sigma_f}{4\tau_s} \cdot \quad (16)$$

Now values for l_m calculated from Equation 16 are significantly smaller than those observed experimentally. Probably this can be attributed to the value of τ_s in the composite being smaller than the values observed in single fibre pull-out tests where there is no fibre-fibre interaction possible and the fibre will be perfectly embedded in the matrix. For the fibre in the composite, an adhesive strength τ_{sc} can be calculated from the observed value of l_m:

$$\tau_{sc} = \frac{d\sigma_f}{4l_m} \cdot \quad (17)$$

If τ_{sc} is smaller than τ_s it is probable that τ_f measured in single fibre tests will be larger than the value (τ_{fc}) applicable to the fibre composite. Assuming the same proportional decrease applies to τ_f as τ_s then

$$\tau_{fc} = \tau_f \frac{\tau_{sc}}{\tau_s} = \frac{\tau_f d\sigma_f}{4l_m\tau_s} \cdot \quad (18)$$

Using Equation 18 in Equation 15, the energy of pull-out can then be written

$$e_{po} = \frac{V_f l_m \tau_f \sigma_f}{12\tau_s} \quad (19)$$

Theoretical values for the pull-out energy were calculated using Equation 19 for epoxy and polyester composites (Table IV). It should be noted that measurements of l_m are a little arbitrary in nature and both τ_s and τ_f measurements are subject to very large scatter. Thus e_{po} can only be estimated approximately. τ_f and τ_s could not be measured for PMMA composites; the mean values obtained in polyester and epoxy composites were therefore used. These estimates are considered reasonable in view of the other approximations involved in the estimation of e_{po}.

For short fibres which pull-out before they reach their tensile strength, Equation 17 will not apply. l_m will be equal to half the fibre length. Because the fibres used were not in bundles and were short, fibre-fibre interaction should be reduced and fibre wetting should be better than for the other samples. Values of τ_f and τ_s measured in single fibre tests were, therefore, used directly in Equation 15 to predict e_{po} for these composites. Results are contained in Table V.

It has been assumed throughout that there is a single crack with pull-out from this crack face. Composites can however show multiple cracking with fragmentation of the brittle matrix. If this were to occur to a large extent (as it may with high fibre concentrations) appreciable amounts of energy could possibly be required. There is therefore another mechanism which could account for the propagation energy. Estimation of the magnitude of the effect is difficult, however.

4.4. Other possible energy absorption mechanisms

One assumption used in calculating the initiation energy was that the presence of fibres effectively blunted the notch and eliminated its stress intensification. Now if we assume that the propagating crack is also blunted, the stress at the crack-tip will be insufficient to continue the failure process without the undamaged section being bent further and absorbing greater flexural energy. Hence effectively we require to provide extra "initiation" energy to enable the crack to continue propagation. For perfect crack blunting of the propagating crack it is shown in Appendix 1 that a contribution to the propagation energy of twice the initiation energy is received owing to this crack-initiating propagation energy.

In an alternative approach [2] a de-bonding energy (i.e. the energy required to failure of the fibre-matrix adhesive bond) was calculated as one contribution to the fibre composite fracture energy. In our treatment such a contribution is

automatically included in the calculated initiation energy term e_i.

On failure, the test pieces acquire kinetic energy and are flung away from the impact tester. The maximum observed speed of the fragments was of the order of 2 m sec^{-1} although most samples did not reach this velocity. Hence at a maximum, the kinetic energy of the fragments (typical weight 2×10^{-3} kg) is 0.004J. This is equivalent to a maximum estimate of 0.3 kJ m^{-2} of sample cross-section. Hence kinetic energy of the fragments is negligible compared to the other calculated contributions.

4.5. Predicted NIS values

To compare with the Charpy notched impact strengths, all of the contributions to work of fracture discussed above must be added together. Individual energy contributions are tabulated and compared to NIS values in Tables IV and V. Adding together $(e_i)_{Th}$ and e_{po} gives a good correlation with NIS values for both very long and very short fibre composite samples. This correlation is contained in Fig. 6 for epoxy and polyester composites and Fig. 7 for PMMA composites. The proposed model for the propagation energy is therefore shown to be adequate for predicting the fibre fracture energy. The postulated crack initiating propagation energy must also be small implying that, although

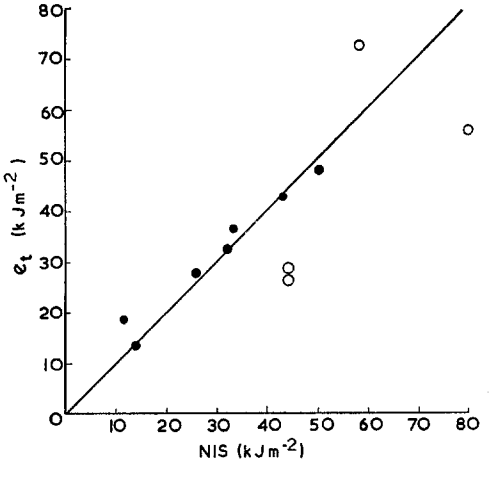

Figure 6 Comparison of theoretical fracture energy e_t and notched impact strength for epoxy and polyester matrices containing continuous uniaxially-oriented fibres (○) and planar random fibres of length greater than 2.5 cm (●).

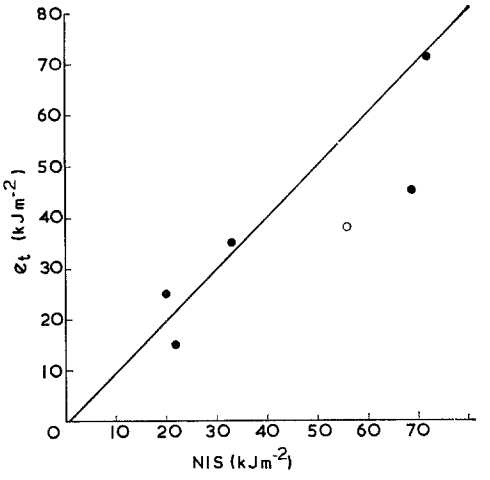

Figure 7 Comparison of theoretical fracture energy e_t and notched impact strength for PMMA matrices containing continuous-uniaxially oriented fibres (○) and planar random fibres of length greater than 2.5 cm (●)

the fibres spread the load away from the notch, they do not effectively blunt the sharp propagating crack. The theoretical work of fracture $(e_t)_{Th}$ will therefore be given by

$$(e_t)_{Th} = (e_i)_{Th} + e_{po}. \tag{20}$$

For long fibres in which $(2L\tau_s/d) \gg \sigma_f$, Equations 14, 19, 11, 12, 3, 13 and 17 are applicable

$$\therefore (e_t)_{Th} = \left(\frac{1}{2u}\right)(F/b)_{Th}\chi_{Th} + \frac{V_f l_m \tau_f \sigma_f}{12\tau_s}$$

i.e.

$$(e_t)_{Th} = \left(\frac{D}{18}\right)\frac{E_c}{E_f^2}\sigma_f^2 + \frac{V_f \tau_f d \sigma_f}{48\tau_s \tau_{sc}} \cdot \tag{21}$$

For very short fibres in which $(2L\tau_s/d) < \sigma_f$, Equations 8, 9, 11, 12, 14 and 15 apply.

Equation 20 becomes

$$(e_t)_{Th} = \frac{L^2\tau_f^2 D E_c}{18d^2E_f^2} + \frac{V_f\tau_f L^2}{12d} \cdot \tag{22}$$

4.6. Predicted unnotched impact strengths

If it is assumed that fibres distribute the stress away from the notch, eliminating its effect entirely, unnotched impact strengths(UNIS) are therefore predicted to be equal to the NIS values. This prediction was verified using a wide range of fibre composites (Fig. 8).

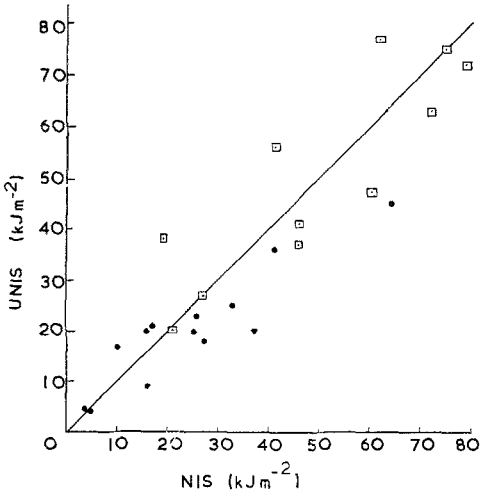

Figure 8 Comparison of unnotched and notched impact strengths of composites containing planar randomly-oriented fibres. (Points ●, L3 Terylene fibres and points □, E glass fibre.) The results are for composites with fibre volume fractions in the range 17 to 45% and fibre lengths in the range 0.06 to 2.5 cm.

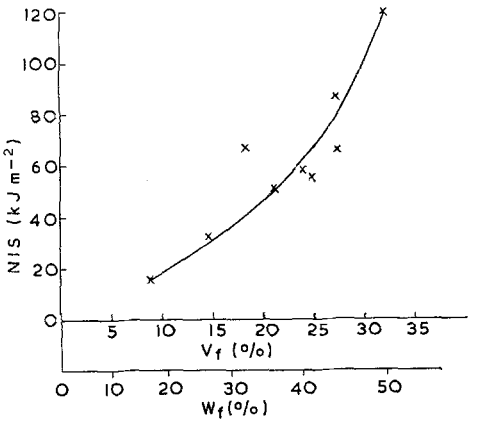

Figure 9 Effect of fibre concentration of 1.3 cm planar randomly oriented glass fibres in PMMA.

5. The effect of composite variables

The impact strengths of a large number of different fibre composites have been predicted successfully using the analysis developed above. Attempts will now be made to predict the effect of the many composite variables studied in this work and the predictions will be compared with experimental data.

5.1. Fibre concentration

For both very short and long fibres, e_i is proportional to the composite modulus E_c. E_c in its turn is proportional to the fibre modulus E_f and volume fraction V_f if E_f is much greater than E_m. Therefore, e_i should be proportional to V_f for glass fibre composites. e_{po} and e_d should also be proportional to V_f. Thus a proportional dependence of NIS upon V_f for glass fibre composites is to be expected from Equation 21. Results for low fibre concentrations are consistent with such a proportional trend (Fig. 9). There is however, a gradual increase in the rate of NIS increase at larger concentrations. The increase above values predicted from a linear relationship is probably caused by an increase in e_{po} resulting from a decrease in τ_{se}, the adhesive strength of the fibre-matrix bond. (Greater fibre-fibre interaction should occur at large V_f values.)

For long polymer fibres, E_c will not be proportional to V_f because E_f is not sufficiently greater than E_m. The anisotropy in fibre modulus properties could also complicate a simple relationship between E_f and E_c. With increase in V_f, experimental results show that E_c decreases for the lower modulus fibres. e_i should therefore decrease with increase in V_f. e_{po} should of course still increase linearly with V_f, so the nett effect will depend upon the relative magnitude of e_i to e_{po}. In fact, in our work, e_i was less than e_{po} for all samples used to investigate the effect of V_f. The observed increase in NIS with V_f (Fig. 10) is therefore consistent with the foregoing analysis. The analysis also predicts that below a critical value of V_f the NIS should increase with decrease in V_f. This need not necessarily be observed however since at low V_f the model used to predict V_f must break down because stress will not be adequately transferred away from the notch.

In summary, all of the trends in NIS observed with fibre concentration are consistent with the proposed theory.

5.2. Fibre length

Provided fibres are sufficiently long to enable the fibre fracture stress to be reached, E_c and l_m should both be independent of length. The model proposed therefore predicts that both e_i and e_{po} will be independent of fibre length. In fact for both Terylene (Fig. 10) and glass fibres (Fig. 11)

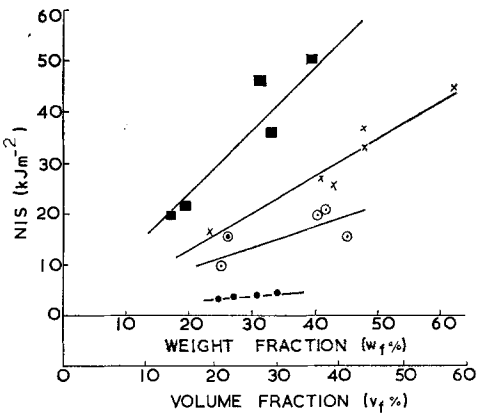

Figure 10 Effect of fibre concentration for planar randomly oriented L3 Terylene fibres in PMMA. Fibre lengths are 0.06 cm (●), 0.6 cm (○), 1.3 cm (X) and 10 cm (■).

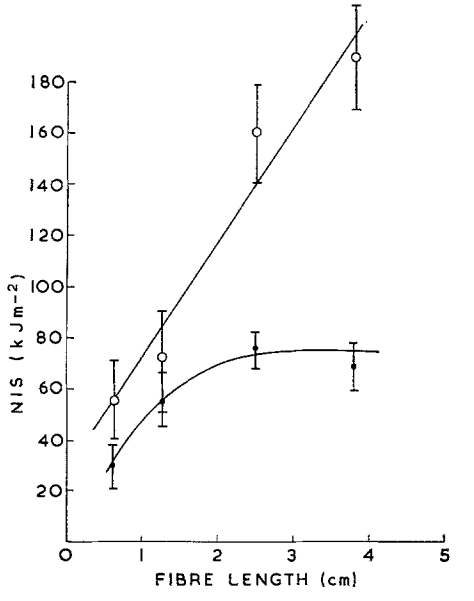

Figure 11 Effect of fibre length on NIS of sized glass fibre bundles in PMMA. Fibre weight fraction = 45%. Points ● are for planar randomly oriented fibres, points ○ are for uniaxial fibres.

significant decreases in NIS were observed with decrease in fibre length even though the observed l_m values were constant for fibre lengths above 0.6 cm, indicating that fibres should be reaching their tensile strength. These results suggest a departure from the proposed model as the fibre length is reduced. (Quantitative agreement with the model was demonstrated using the longest fibre samples (Section 4.5).) In the calculation for e_i it is assumed that all fibres reach their tensile strength. Even with long fibres however, there will always be some fibres with ends sufficiently close to the position of maximum stress that they will pull-out before the fibre tensile strength has been reached. The number which do not reach their tensile strength, will decrease with increase in fibre length. A decrease in e_i with decrease in fibre length is therefore explicable. At very long fibre lengths the effect should be negligible and agreement with the simple theory is expected.

The maximum length of a fibre that can pull-out, l_m, was calculated from Equation 5 with $\sigma_{fp} = \sigma_f$. All longer lengths should fracture rather than pull-out. Ideally these should fracture at the point of largest stress and not contribute to the work of pull-out. On this basis e_{po} for long fibres would be in error since Equation 21 assumes a uniform distribution in l between zero and l_m. The presence of flaws in fibres will however contribute to a distribution in l without affecting l_m. The agreement between theory and experiment for long fibres justifies the assumption of a uniform distribution.

With very short fibres which do not reach their tensile strength, the theory predicts the small NIS values obtained. In this region it would be expected that increase in fibre length L would cause an increase in NIS, NIS being proportional to L^2. Increase in the frictional shear coefficient τ_f and reduction in diameter should also increase the NIS provided changes are not large enough to cause a significant amount of fibre fracture. This in turn requires that the maximum fibre stress at pull-out be smaller than the fibre tensile strength, i.e.

$$\frac{2L\tau_s}{d} \leqslant \sigma_f \ .$$

5.3. Fibre diameter and number of filaments per bundle

Two sets of data were obtained for a study of the effect of diameter and number of filaments per bundle on the NIS of glass fibre/PMMA composites, one using short (0.25 in.) fibres, the other using long (4 in.) fibres.

The short fibres were supplied with a commercial size suited for use with vinyl matrix polymers. In fact, the size bound the fibres so well that each bundle acted as a single entity. The method of bundle formation provided approximately rectangular bundles. During com-

TABLE VI 0.6 cm random glass fibre/PMMA composites. Effect of fibre diameter d, number of filaments per bundle n, and bundle dimensions on the NIS value at a fibre weight fraction of 45%

Sample reference	n	d (μm)	Bundle width (μm)	Bundle thickness (μm)	NIS* (kJ m^{-2}) (± 5 kJ m^{-2})
Q	816	23	2030	182	31
M	816	18	1180	138	38
K	816	14	1560	113	33
G_1	816	10	1550	89	39
K	816	14	1560	113	33
K-S2	408	14	1280	81	43
K-S4	204	14	780	82	50
K-S8	102	14	540	61	62

*NIS values were interpolated from graphs of the variation of NIS with fibre weight fraction

posite fracture there was little visual sign of fibre fracture; bundles appeared to pull out of the matrix as a complete unit as the crack propagated. One range of samples had a fixed number of fibre filaments per bundle and varying fibre filament diameter. The thickness of the bundle was almost constant for all of these samples and the width (which was much greater than the thickness) varied. There was no significant variation in NIS at a given fibre concentration between any of these samples (Table VI). The other range of short fibre samples had a variable number of filaments per bundle, with constant filament diameter being used in each case. The bundle thickness and width reduced systematically with reduction in number of filaments. A steady increase in NIS was observed with decrease in the number of filaments (Table VI).

Now observation of the fracture surfaces showed that failure is most certainly initiated by fibre pull-out rather than fibre fracture. Analysis analogous to that presented for very short round fibres will be applicable, but in this case the pull-out of rectangular entities must be considered. It has been demonstrated in Appendix 2 that for bundle thickness much less than the width, the average fibre stress at pull-out is given by

$$\sigma_{fp} = \frac{\tau_f l_m}{p} \cdot \qquad (23)$$

where l_m is the maximum pull-out length and p is the bundle thickness. The work of pull-out for a short fibre sample of length L is given by

$$e_{po} = \frac{V_f \tau_f L^2}{12p} \cdot \qquad (24)$$

Thus the theory predicts increase in both initiation and propagation energies with decrease in bundle thickness, provided that bundle thickness is still sufficiently large so that there is complete fibre pull-out. The observed NIS trends and independence of NIS of bundle width (Table VI) are, therefore, consistent with the theory.

The glass fibres used to make long random fibre composites were less tightly bonded. Observations of the fracture surface indicated that the fibres were to a first approximation acting individually, i.e. the matrix had penetrated the fibre bundles. With long fibres (Equation 21), it would be expected that e_i would be independent of diameter and that e_{po} would increase in proportion with fibre diameter. The increase in NIS with increase in diameter (Table VII) is therefore expected. For these samples at 30% wt/wt fibre, the theory predicts e_i to be 26 kJ m^{-2}. Predicted e_{po} values are 2.6 kJ m^{-2} for the 4 μm diameter fibre and 7.4 kJ m^{-2} for the 13 μm diameter fibre. The theoretical increase in NIS is, therefore, from 29 to 35 kJ m^{-2} and is consistent with the experimental values of 29 and 41 kJ m^{-2}.

The effect of using very large fibre diameters was studied using Terylene fibres. The fibres used in the comparison had comparable tensile properties but filament diameters of 247 and 23 μm. Although the smaller fibre came in a bundle of 190 filaments, each filament had separated in composite fabrication due to the absence of inter-filament bonding. Results are therefore directly comparable. It was found that fibre fracture and pull-out occurred for the small diameter fibres whereas no fibre fracture was observed for the large "macro fibre". In the latter case partial pull-out occurred and the

fibres bridged the gap between the two separate matrix segments (see Fig. 1c). Equation 22 and not Equation 21 of the theory would therefore be expected to apply. The sample is in the region for which increase in diameter leads to a reduction in NIS. The experimental observation of similar NIS values for both macro-fibres and small diameter fibres (Table VII) is not therefore inconsistent with the analysis. The NIS value of the macro-fibre composite cannot be accurately predicted because of uncertainty in l. Nevertheless, reasonable values of l and τ_f can be selected which are consistent with Equation 22 and the NIS value.

5.4. Fibre type

NIS results for all of the different types of fibre used have already been shown to be consistent with the theory. Since fibre tensile strength, modulus and adhesive bonding vary considerably with fibre type, these data give the most definitive proof of the usefulness of the theoretical approach presented.

5.5. Matrix toughness

Increase in matrix toughness occurred as a result of increased strain at fracture for the matrices studied. The constant NIS values obtained with random fibres in matrices of varying toughness (Fig. 3) was therefore taken as an indication that fibre fracture or interface failure was controlling fracture. Equation 21 confirms that the other changes in matrix properties accompanying the increased toughness would not be expected to alter greatly the predicted NIS. For example, a smaller matrix modulus does not greatly affect the glass-fibre composite modulus, nor are changes in the adhesive bond with altered chemical composition likely to alter τ_f.

5.6. Temperature

The tensile strength of E glass fibre decreases slightly with increase in temperature [16]. Any decrease in tensile modulus (which also controls E_c) should be correspondingly small. From Equation 22 the essentially constant NIS of short glass fibre composites tested at different temperatures (Fig. 12) therefore implies that the interfacial adhesion τ_f is independent of temperature, a surprising conclusion in view of the different expansion coefficients of the fibre and matrix. For long fibre composites the pull-out energy is more sensitive to any change in tensile strength (Equation 21) and so the slight decrease

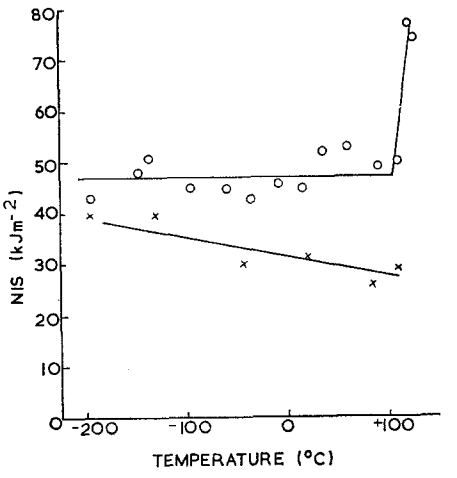

Figure 12 Effect of temperature on the NIS of composites of PMMA containing planar randomly-oriented glass fibres. Points ○ are for 0.6 cm long sized fibre bundles and points X are for 10 cm long water-sized fibres.

observed with increase in temperature (Fig. 12) can be explained solely by the reduction in fibre tensile strength.

Prediction of the temperature variation of NIS values for polymer fibre composites is complicated by variation in the fibre tensile properties. Expected trends in σ_f and E_f were obtained from Technical Service data sheets of similar commercial fibres. For all fibres a decrease in σ_f and E_f with temperature is expected. E_c will also decrease with temperature in association with the decrease in E_f and E_m. For long Terylene fibres, e_i is expected to decrease very slightly due to an expected decrease in σ_f^2/E_f with increase in temperature. On the other hand, l_m and e_{po} will decrease more drastically due to the decreases in σ_f with temperature. The predicted decrease in l_m was apparent from visual examination of fracture surfaces of samples tested at 20 and 80°C. The expected decrease in e_t with temperature increase resulting from the decrease in e_{po} is indicated in Fig. 13 and 14, together with the experimentally observed variation of NIS. The decrease in NIS up to 100°C can be quantitatively predicted from the decrease in e_{po}.

Surprisingly, cotton and nylon fibre composites showed increases in NIS with increase in temperature (Fig. 15). The increase cannot be predicted theoretically with the simple arguments used for Terylene and glass fibres. It is necessary to assume additional effects such as a change in

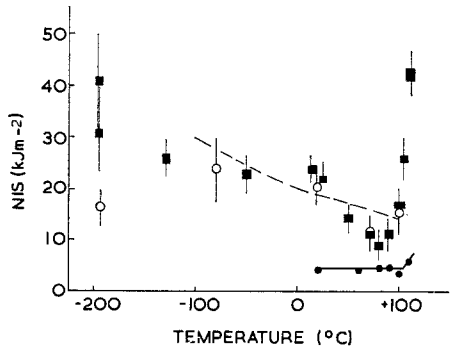

Figure 13 Effect of temperature on the NIS of composites of PMMA containing planar randomly oriented L3 Terylene fibres. Fibre lengths are 0.06 (points ● – W_f = 31%), 0.6 cm (points ○ – W_f = 41%) and 10 cm (points ■ – W_f = 19%). The theoretical curve for the 0.6 cm fibre length is dotted.

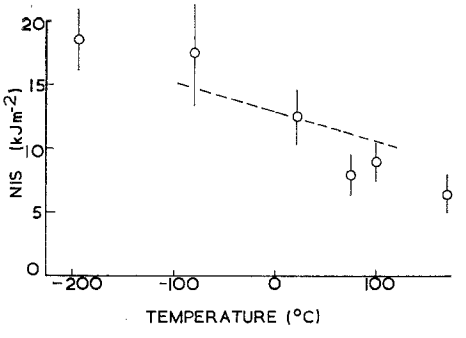

Figure 14 Effect of temperatures on the NIS of a composite of polyester containing 10 cm long, planar randomly oriented L3 Terylene fibres. The theoretical curve is dotted.

adhesion with temperature. This difference for nylon and cotton fibres is not understood.

For all composites with PMMA matrices at temperatures above the expected glass transition temperature of 105°C, an increase in NIS was observed. No such increase was observed with polyester matrices (Fig. 14). The increase might therefore result from an alteration in the nature of fracture in the rubbery matrix. For example, with a rubbery matrix, the crack initiating propagation energy (Appendix 1) could become important.

5.7. Uniaxially oriented fibres

In the model used for the theoretical approach, no effect of fibre orientation would be expected, except in terms of an effect upon E_c, provided too many fibres were not oriented near the crack

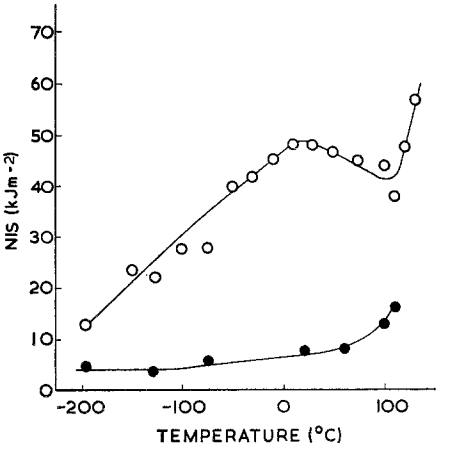

Figure 15 Effect of temperature on the NIS of composites of PMMA containing planar randomly-oriented fibres; points 0 are for 30% of 10 cm nylon fibres and points ● for 17% of 5 cm cotton fibres.

TABLE VII Long (10 cm) random fibre/PMMA composites. Effect of fibre diameter d and number of filaments per bundle n on the NIS value at a fibre weight fraction of 30%

Fibre type	n	d (μm)	NIS* (kJ m^{-2}) (±5 kJ m^{-2})
"E" glass	102	5	28 ± 5
	1224	4	30 ± 5
	204	13	60 ± 8
	408	13	41 ± 5
H type	190	23	80 ± 15
Terylene	1	247	65 ± 15

*NIS values were interpolated from graphs of the variation of NIS with fibre weight fraction

plane. Composites with both continuous and discontinuous uniaxially oriented fibres have been compared with the theory and excellent quantitative agreement obtained (Table IV and Figs. 6 and 7).

For fibre systems in which failure did not involve crack propagation across the width, the theoretical model used in this paper will not be applicable.

6. Damage initiation observations

With unfilled PMMA, samples tested were either completely undamaged or completely fractured, depending upon whether the pendulum energy was above or below a critical value. Repeated impacts at energies below the critical energy did not cause any visible permanent damage and

samples could be subjected to many impacts without fracture.

For fibre composites, on the other hand, some permanent damage was observed at pendulum input energies considerably below the energy required for complete fracture. The observed damage was recorded as a function of the input energy for a wide range in fibre composites. Of course, there was a considerable variation between different samples cut from the same fibre composite sheet but the typical damage occurring at each input energy was recorded. It was found that for most samples the range over which permanent damage occurred changed in approximate proportion to the changes in UNIS. With input energies up to about 10% of the fracture energy no damage was detected even after many successive impacts. Above this level, however, some permanent damage consisting of slight de-bonding of the fibre-matrix interface was observed. Successive impacts with input energies of about 25% of the fracture energy eventually produced a hair-line crack in the tensile surface which grew in following impacts and eventually led to failure after many impacts. A single impact with an input energy about 50% of the fracture energy caused a crack in the tensile surface. After a few more impacts complete failure by crack propagation had been induced. The observations are consistent with theoretical and tensometer measurements of the crack initiation energy which for most samples was found to be about 33% of the total fracture energy.

An exception to the above behaviour was observed with random cotton fibre composites. These required the input energy to be a larger proportion of the fracture energy before damage occurred. For example, impacts with 33% of the fracture energy caused no visible damage and 60% caused only slight de-bonding. There was again a correlation between the theoretical crack initiation energy and that measured with the tensometer (62% of the fracture energy) and the energy of the pendulum for crack initiation in the damage initiation impact test.

7. Discussion

The behaviour under impact of many types of fibre composite has been recorded in this paper. In general, permanent damage occurred for a wide range of impact energies below the fracture energy. At the lowest energies, the permanent damage consisted of de-bonding of the fibre-matrix interface. Higher impact energies caused cracking on tensile surfaces and with increased energy or repeated impacts the crack length grew. The range of energy over which permanent damage occurred has been approximately defined by two energies, the fracture energy and the energy to just initiate a crack on the tensile surface of a sample deformed in a flexural manner during impact. Some permanent damage such as fibre-matrix de-bonding will occur below the crack initiation energy. Nevertheless, for applications where surface finish is important, a comparison between crack initiation energies of materials will be useful as a first approximation. Now for the polymer matrices studied in this report, the unfilled polymer shows no damage prior to fracture, i.e. the crack initiation energy is very close to the fracture energy. The composite crack initiation energies were very little better and frequently worse than the crack initiation energy of the unfilled polymer. Fibre composites will therefore be no better and often worse than unfilled polymers when used for rugged applications demanding maintenance of good surface finish. On the other hand, fibre composites absorb a large amount of energy after the first permanent damage has occurred. Fibre incorporation is, therefore, ideal for localizing damage which would otherwise be catastrophic.

Two models have been developed for predicting the crack initiation energy, notched impact strength and unnotched impact strength of fibre composites. One is applicable to long fibre composites which have been shown to fail when the fibres reach their tensile strength. The other is applicable to short fibre composites for which failure is controlled by fibre pull-out. It is argued that the expressions derived for tensile strength, failure strain and fracture energy should be independent of the fibre orientation provided that only a small proportion of fibres are oriented near to the crack propagation plane. Extra energy absorption mechanisms are therefore not necessary to explain the similar fracture energies of uniaxial and random fibre composites [10]. Any differences in failure properties with fibre orientation are predicted to be due to variations in composite modulus with fibre orientation. (Composite modulus is one of the factors included in the deduced expressions.)

Limited data obtained with short random fibre composites are consistent with the short fibre model. They are not sufficient to verify the validity of the model however. Indeed it is

certain that the model will not apply with the shortest fibres since it assumes that the fibres transfer stress away from the stress-concentrating notch which is not possible for very short fibres. Short fibre-reinforced plastics are widely used since fibre length is often restricted by the fabrication process (e.g. injection moulding). Further evaluation of the applicability of the proposed short fibre model will, therefore, be an important future area of work.

Extensive data obtained with planar random and uniaxial long fibre composites has been used to verify the validity of the long fibre model for the notched and unnotched impact strengths. Perhaps surprisingly, it was found that the failure stress used for the model could be calculated on the basis of uniform strain in fibre and matrix. This contrasts with more complicated methods of approach which have been attempted for such systems [5]. The maximum stress and strain were used to calculate a crack initiation energy which correlated well with tensometer measurements of the energy to initiate a crack and impact damage initiation measurements.

The large crack propagation energy of the fibre composites was found to be composed entirely of the work required to pull fibres out from opposite faces after failure. In summary, therefore, the successful application of the model indicates that the high notched impact strength of composites is due to redistribution of stress away from the stress-concentrating notch, the extra stress that can be held by the fibres relative to the matrix and the work of pulling fibres out from the matrix.

The model developed will be of use in optimization of composite variables for maximum toughness. The fracture energy increases with increase in fibre tensile strength and volume fraction. The matrix toughness has no effect at all for planar random fibres and uniaxially-oriented fibres and only a minor effect in exceptional cases. Other variables which have been shown to control the composite notched impact strength are composite modulus, fibre length, effective fibre diameter and the coefficient of friction during fibre pull-out from the matrix. Optimum values of length, diameter and adhesion are interrelated. At a given fibre length L, low enough τ_s or large enough d values can be selected so that the stress for pull-out, $2\tau_s L/d$, is smaller than σ_f the fibre tensile strength. All fibres then pull-out. The frictional coefficient after bond failure τ_f and diameter d control the fracture energy for this mode of failure. Increases in τ_f and decreases in d cause increases in both initiation and propagation energies. For all of the fibre-matrix systems studied, similar τ_f values were observed. Hence adjustment of τ_f may not be easy. d on the other hand can be easily increased by bonding the individual filaments together with a size to give a macro-fibre. If either τ_s is increased or d is decreased too much, then $2\tau_s L/d$ will eventually exceed σ_f and some fibres will fracture. When most fibres in the composite fracture before pull-out (i.e. when $2\tau_s L/d \gg \sigma_f$) then increase in d and reduction in L and τ_f would be expected to give an increase in propagation energy. With the wide range of composites studied the expected trend in NIS was not observed. For example, NIS values decreased with decrease in L. It is postulated that the observed trend is probably due to the dominating influence of a reduction in e_i with decrease in fibre length, the effect being due to a proportion of the fibres not reaching their tensile strength at composite failure. The proportion of such fibres will decrease with increase in fibre length and is probably only significant at the largest fibre lengths used. In summary therefore, although a simplified theory may predict optimum values for τ_s, L and d such that

$$2\tau_s L/d = \sigma_f$$

in practice, much larger values for $2\tau_s L/d$ may be required.

The above discussion has been concerned with adjusting parameters to increase the total fracture energy. However, use of fibre composites is often restricted by the low threshold energy for damage initiation. Future theoretical and practical work could therefore be usefully focused on increasing the energy required for fibre-matrix de-bonding and crack initiation.

Appendix 1

Energy required to maintain blunted crack propagation

If, after crack initiation in a fibre composite, the fibres effectively blunt the propagating crack so that its stress intensification effect is eliminated continued crack propagation will not occur unless extra flexural energy is supplied to the undamaged portion of the sample. This is necessary to keep the tensile force at the crack tip equal to the failure stress. For perfect crack

blunting the extra flexural energy can be easily related to the flexural energy required to initiate crack propagation.

To calculate the crack initiation energy, the Charpy sample can be treated as an unnotched beam of depth u (u being the distance below the notch in the actual sample).

Crack initiation occurs when the stress at the surface of the beam of depth u is equal to the failure stress σ_c. The tensile stress in the beam decreases linearly with distance from the top surface to a value of $-\sigma_c$ on the compressive face.

The energy dE in an element distance s of the neutral axis is given by

$$dE = \int_0^{\epsilon_s} \sigma b(ds).\ D\ d\epsilon$$

where ϵ_s is the strain in the element at s at failure, b is the sample width and D the span.

If we assume a linear relationship between stress σ and strain ϵ then

$$\epsilon = \sigma/E_c.$$

Hence we can write

$$dE = \int_0^{\sigma_s} \frac{bD(ds)}{E_c}\,\sigma\,d\sigma = \frac{Db(ds)}{2E_c}\,\sigma_s^2\,. \quad (25)$$

Now

$$\sigma_s = s\sigma_c/(u/2)$$

$$\therefore \quad dE = \frac{2bD(ds^2)s\sigma_c^2}{E_c^2u^2}\,.$$

The total energy in the beam at crack initiation is therefore given by

$$E_I = 2\int_0^{u/2} \frac{2bL\sigma_c^2}{E_c\,u^2}\,s\,ds$$

$$\therefore E_I = \frac{Lub\sigma_c^2}{6E_c}\,. \quad (26)$$

If the propagated crack is perfectly blunted, all elements such as the one at s must be taken to a stress σ_c. The total energy absorbed due to crack blunting (including E_I) in element s is, therefore, given by

$$dE_b = \frac{bL(ds)\sigma_c^2}{2E_c}$$

(using $\sigma_s = \sigma_c$ in Equation 25). Hence the total energy absorbed owing to crack blunting

$$dE_b = \frac{bL\sigma_c^2}{2E_c}\int_{u/2}^{u/2} ds$$

$$= \frac{Lub\sigma_c^2}{2E_c}$$

$$= 3E_I.$$

Hence this model proposed an extra energy absorption mechanism during propagation of a crack through a fibre composite. The magnitude of the energy absorbed will depend upon how effectively the fibres can blunt the propagating crack. The maximum possible energy absorbed is predicted to be twice the energy required to initiate a crack.

Appendix 2

Pull-out of rectangular fibres

Consider rectangular cross-section fibres of length L, width q and thickness p. The stress σ_{fp} in the fibre necessary to break the fibre-matrix adhesive bond and start fibre pull-out will be given by

$$\sigma_{fp}\,p\,q = l.2q\,\tau_s \quad (28)$$

for a length l resisting pull-out. Equation 1 assumes that $q \gg p$.

Hence the average pull-out stress when there is a distribution in pull-out length from zero to l_m will be given by

$$\sigma_{fp} = \frac{\tau_f l_m}{p} \quad (29)$$

(τ_f replaces τ_s as discussed in Section 4.1.1.).

When the fibre is pulling out and still has a length χ to pull-out, the force in the fibre

$$f = 2q\,\chi\,\tau_f.$$

The work done in moving the fibre a distance $d\chi$ at the point χ is equal to

$$dW = -2q\,\tau_f\chi d\chi$$

The total work to pull out this single fibre of total pull-out length l is given by

$$W(l) = 2q\,\tau_f\int_0^l \chi d\chi$$

$$= q\,\tau_f l^2.$$

Now in a composite we have a distribution in l from zero to $L/2$. If $n\,dl$ is the number of fibres in the range l to $l + dl$, the total work done for the composite

$$e_{po} = \int_0^{L/2} q\tau_f l^2 n \, dl$$

$$= Nq\,\tau_f \frac{\int_0^{L/2} l^2\, l}{\int_0^{L/2} dl}$$

where N is the total number of fibres in the sample across sectional area A.

$$\therefore \qquad e_{po} = \frac{Nq\tau_f L^2}{12} \, .$$

Now

$$\frac{Npq}{A} = V_f,$$

hence work of pull-out (per unit sample cross-section) $= \dfrac{V_f \tau_f L^2}{12p}$.

Acknowledgements

The authors are extremely grateful to N. M. Singh for his experimental assistance throughout the course of the work. Scanning electron microscopy was kindly carried out by Dr R. T. Murrey. The help of Dr J. E. Macintyre (ICI Fibres Division) in suggesting and supplying suitable polymer fibres is greatly appreciated. Other fibres were kindly supplied by Fibreglass Ltd, Owens-Corning Fiberglas Ltd, English Sewing Ltd and DuPont Ltd.

References

1. P. I. VINCENT, "Impact tests and service performance of thermoplastics" (The Plastics Institute London, 1971).
2. J. O. OUTWATER and M. C. MURPHY, 24th Annual Conference of Reinforced Plastics/Composites Division of SPI, paper 11C (1969).
3. J. H. DAVIES, *Plastics and Polymers* **39** (1971) 137.
4. H. BRODY and I. M. WARD, *Polymer Eng. Sci.* **11** (1971) 139.
5. J. K. LEES, *ibid* **8** (1968) 195.
6. A. KELLY, *Proc. Roy. Soc.* **A319** (1970) 95.
7. A. H. COTTRELL, *ibid* **A282** (1964) 2.
8. N. L. HANCOX, *Composites*, **3** (1971) 41.
9. M. R. PIGGOTT, *J. Mater. Sci.* **5** (1970) 669.
10. P. HING and G. W. GROVES, *ibid* **7** (1972) 427.
11. G. ALLEN, M. J. BOWDEN, D. J. BLUNDELL, F. G. HUTCHINSON, G. M. JEFFS and J. VYVODA, ICI/Manchester University Joint Laboratory report (1971), to be published.
12. G. ALLEN, M. J. BOWDEN, D. J. BLUNDELL, G. M. JEFFS, J. VYVODA and T. WHITE, ICI/Manchester University Joint Laboratory report (1971), to be published.
13. J. D. EMMERSON, to be published.
14. G. V. SHIRIAJEVA and G. D. ANDREVSKAYA, *Sov. Plastics* **4** (1962) 40.
15. D. C. WEST, "Experimental Mechanics" (Instron Application Series PC-18, 1964).
16. J. H. WESTBROOK, *Physics Chemistry Glasses* **1** (1960) 32.

Received 3 April and accepted 15 June 1973.